

Reactive Rayleigh-Taylor turbulent mixing: a one-dimensional-turbulence study

E. D. GONZALEZ-JUEZ*[†], A. R. KERSTEIN[†], and D. O. LIGNELL[‡]

[†]Combustion Research Facility, Sandia National Laboratories, Livermore, California 94551, USA

[‡] Department of Chemical Engineering, Brigham Young University, Provo, Utah 84602, USA

(Received 9 November 2011; in final form 13 September 2012; first published online ????)

We study the problem of reactive Rayleigh-Taylor turbulence in the Boussinesq framework using one-dimensional-turbulence (ODT) simulations. In this problem a reaction zone between overlying heavy/cold reactants and underlying light/hot products moves against gravity. First, we show that ODT results for global quantities in non-reactive Rayleigh-Taylor turbulence are within those from direct numerical simulations (DNS). This comparison gives us confidence in using ODT to study unexplored flow regimes in the reactive case. Then, we show how ODT predicts an early stage of reactive Rayleigh-Taylor turbulence that behaves similarly to the non-reactive case, as observed in previous DNS. More importantly, ODT indicates a later stage where the growth of the reaction zone reduces considerably. The present work can be seen as a step towards the study of supernova flames with ODT.

Keywords: Rayleigh-Taylor; Turbulence; Numerical simulations; One-dimensional-turbulence model

1. Introduction

Rayleigh-Taylor mixing is a canonical flow problem relevant to myriad applications, such as mixing in the atmosphere, ocean, rivers, and estuaries, the evolution of stars, and inertial confinement fusion (e.g. Sharp 1984). Consequently it has been extensively studied with theory (cf. Abarzhi and Rosner 2010 for a recent review), experiments (e.g. Linden *et al.* 1994, Ramaprabhu and Andrews 2004, Banerjee *et al.* 2010), and computer simulations (e.g. Cook *et al.* 2004, Ristorcelli and Clark 2004, Dimonte *et al.* 2004, Cabot and Cook 2006, Mueschke and Schilling 2009, Vladimirova and Chertkov 2009, Boffetta *et al.* 2010). On the other hand, less attention has been given to the problem of Rayleigh-Taylor mixing occurring with chemical or nuclear reactions. This flow is relevant, for example, in large-scale fires (e.g. Tieszen 2001) and in supernova flames (e.g. Zingale *et al.* 2005). One framework for the study of this problem considers an incompressible (Boussinesq) flow with a simple reaction, and seeks a very basic description of the flow (Chertkov *et al.* 2009, Biferale *et al.* 2011). In this framework there is no heat release nor its accompanying fluid volumetric expansion. However, this framework is useful for the analysis of flame-turbulence interactions in an idealized way (e.g. Vladimirova

*Corresponding author. Email: estebandgj@gmail.com

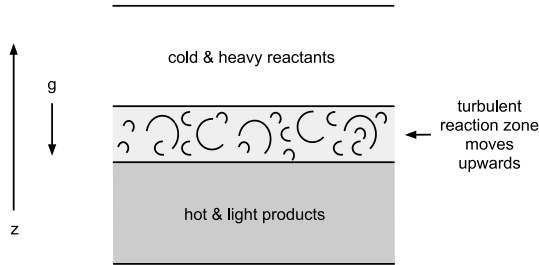


Figure 1. Schematic of the reactive Rayleigh-Taylor problem.

et al. 2003, Chertkov *et al.* 2009). The present work follows this approach. Another framework considers a mildly compressible (low-Mach-number) flow, and uses a reaction and a equation of state that seek to emulate real supernova flames (e.g. Bell *et al.* 2004, Zingale *et al.* 2005). Regarding this latter framework, the current study can be seen as a step towards the simulation of supernova flames with a novel turbulence model, described shortly.

In reactive Rayleigh-Taylor, the mixing layer or reaction zone moves against gravity into overlying cold and heavy reactants, leaving behind hot and light products, cf. figure 1. Whenever a portion of heavy fluid is surrounded by light fluid, or vice versa, buoyancy acts and enhances the mixing, increasing the thickness of the reaction zone. What the reactions do is to convert mixed fluid into products, in other words, they separate light and heavy fluids. Therefore, an interesting question to address is the following one (Chertkov *et al.* 2009): Can this separation process dominate buoyancy in a way that the thickness of the mixing layer stops growing? Addressing this question is the primary objective of the present work. For this purpose it is necessary to consider layers of light and heavy fluid of very large horizontal extent (transverse to gravity) and of thickness much larger than that of the reaction zone.

Undertaking this objective with experiments is very challenging. Moreover, doing so with direct numerical simulations (DNS) is computationally expensive, because they would need a large computational domain and large simulation runtimes. Hence a more convenient approach is to use a simplified model. A recent model of Rayleigh-Taylor turbulence has been able to capture many of its features (Abarzhi *et al.* 2007). However, to address the above question, this model would require closure for the reaction term in its governing equations, i.e., turbulence-reaction interactions need further modeling. This issue can be circumvented with the so-called one-dimensional-turbulence (ODT) model (Kerstein 1999a). Therefore, ODT is used in the present work.

ODT simulations are fully resolved, unsteady, stochastic simulations that emulate Navier-Stokes turbulence. They possess two key features. First, the properties of the flow reside on a one-dimensional (1D) domain. This 1D formulation allows full resolution of the interaction between large scales and molecular transport scales with computationally affordable simulations. However, such a 1D formulation restricts the application of ODT to horizontally homogeneous flows, like the one considered here. Second, because vortical overturns cannot occur on a 1D domain, turbulent advection is represented using a stochastic mapping process. In comparison, while Reynolds-averaged Navier-Stokes simulations and large-eddy simulations model the small-scale phenomena and retain the 3D representation of the flow, ODT resolves all the scales of motion but models 3D turbulence. Hence ODT cannot capture geometrical effects

and coherent flow structures, other than the so-called eddy events of ODT.

ODT has been able to reproduce a variety of turbulence phenomena with a concise representation of the interaction between molecular transport, advection, and buoyant forcing (Kerstein 1999a, Kerstein *et al.* 2001). Some examples of flows of interest in geophysics and astrophysics that have been simulated with ODT are Rayleigh-Bénard convection (Wunsch and Kerstein 2005), vertical slot convection (Dreeben and Kerstein 2000), sheared-stratified turbulence (Wunsch and Kerstein 2001, Gonzalez-Juez *et al.* 2011b), double-diffusive convection (Kerstein 1999b, Gonzalez-Juez *et al.* 2011a), penetrative convection (Kerstein 1999a), the atmospheric boundary layer (Kerstein and Wunsch 2006), and buoyancy-reversal flows (Wunsch 2003). However, the Rayleigh-Taylor problem has not previously been studied with ODT. Thus, the secondary objective of the present work is to address the following question: How do ODT results for (non-reactive) Rayleigh-Taylor turbulence compare with those from DNS?

The paper is organized as follows. Section 2 describes the reactive Rayleigh-Taylor problem and the ODT model used for the present work. This ODT model is explained in more depth elsewhere (Kerstein 1999a, Kerstein and Wunsch 2006, Gonzalez-Juez *et al.* 2011a). Then, section 3 addresses our secondary objective and compares ODT results of non-reactive Rayleigh-Taylor turbulence with those of the DNS of Vladimirova and Chertkov (2009). This section will show that ODT results for global quantities compare fairly well with those from the DNS. Section 4 deals with our primary objective and shows that ODT predicts a regime in reactive Rayleigh-Taylor turbulence where the growth of the thickness of the reaction zone reduces considerably at later times.

2. Model description

2.1. Rayleigh-Taylor problem

The Rayleigh-Taylor problem consists of a layer of cold/heavy fluid with density ρ_H that is mixing with an underlying layer of hot/light fluid with density ρ_L under the influence of gravity g , here directed downwards. A schematic of this problem is shown in figure 1. The domain is unbounded in the horizontal directions, but bounded in the vertical one. Its vertical size is denoted L . The Boussinesq approximation is invoked by assuming a small density difference $\rho_H - \rho_L$, and a linear dependence between temperature and density differences. A temperature variation variable, defined as $T = (\rho_H - \rho)/(\rho_H - \rho_L)$, is $T = 0$ in the cold fluid, $T = 1$ in the hot fluid, and $0 < T < 1$ in the mixed fluid. Hereinafter T is simply called temperature. In the reactive case, the cold fluid is the reactant, and the hot one represents the products. The mixed fluid is converted into products according to the reaction $R = 4T(1 - T)\tau_R^{-1}$, where τ_R is the reaction time scale. In the non-reactive case, there is no reaction, i.e. $\tau_R = \infty$. Three parameters characterize this flow: the Atwood number $A = (\rho_H - \rho_L)/(\rho_H + \rho_L)$, which is $A \ll 1$ under the Boussinesq approximation; the Prandtl number $Pr = \nu/\kappa$, where ν is the viscosity of the fluids, and κ is the heat diffusivity between cold and hot fluids; and the ratio t/τ_R with t being time. A Prandtl number of unity is used.

2.2. Overview of ODT

In ODT the velocity vector u_i and temperature T are defined in a 1D domain along the vertical coordinate z . ODT time advances u_i and T in two steps. First, it integrates in time 1D diffusion equations for u_i and a 1D reaction-diffusion equation for T . Second, ODT modifies u_i and T through a stochastic process representing turbulent advection. This stochastic process consists of a random sequence of vortical overturns or eddy events. The process is specified by, firstly, defining the operations performed during an eddy event and, secondly, defining the sampling of these events, i.e. the rules governing the time scale τ , length scale l , and location z_0 of the eddy events. These operations and sampling rules are discussed next.

2.3. Operations during an eddy event

An eddy event consists of two operations. One is a triplet mapping of u_i and T representing the vertical displacement of fluid elements by a notional eddy. The second is a modification of u_i representing the energy redistribution between velocity components induced by pressure and the effect of buoyancy forces. These operations are represented symbolically as

$$u_i(z) \rightarrow u_i(f(z)) + c_i K(z), \quad T(z) \rightarrow T(f(z)), \quad (1)$$

where the (continuous) triplet mapping operation $f(z)$ is defined by

$$f = z_0 + \begin{cases} 3(z - z_0), & \text{if } z_0 \leq z \leq z_0 + l/3, \\ 2l - 3(z - z_0), & \text{if } z_0 + l/3 \leq z \leq z_0 + 2l/3, \\ 3(z - z_0) - 2l, & \text{if } z_0 + 2l/3 \leq z \leq z_0 + l, \\ z - z_0, & \text{otherwise,} \end{cases} \quad (2)$$

and the addition of $c_i K(z)$ represents velocity changes due to pressure gradients and buoyancy forces. According to this prescription, fluid at location $f(z)$ is moved to location z by the mapping operation, thus defining the map in terms of its inverse $f(z)$.

The effect of the triplet map on a flow property profile defined in $[z_0, z_0 + l]$ is to replace the profile with three compressed images of the original, with the middle image flipped. This is how the compressive and rotational motions observed in turbulent flows are represented in ODT (Kerstein 1999a). The triplet map is adopted because it is the simplest map satisfying the following physical requirements: all moments of the flow properties are preserved by the map, i.e. $\int_0^L u_i^n(z) dz$ and $\int_0^L T^n(z) dz$ are preserved; property profiles remain continuous; and changes in the property gradients of order greater than one are prevented (Kerstein 1999a).

The function $K(z)$ in (1) is defined as $K(z) = z - f(z)$ and represents the vertical displacement of fluid elements induced by a triplet map. The constants c_i in (1) are given by

$$c_i = \frac{27}{4l} \left[-u_{i,K} + \text{sgn}(u_{i,K}) \sqrt{\frac{1}{3} \left(\sum_i u_{i,K}^2 + \frac{8}{27} gl T_K \right)} \right], \quad (3)$$

where the summation is over the three velocity components, sgn is the sign function, and

$$u_{i,K} = \frac{1}{l^2} \int_0^L u_i(f(z)) K(z) dz, \quad (4)$$

$$T_K = \frac{1}{l^2} \int_0^L T(f(z))K(z) dz . \quad (5)$$

It is useful to think of $u_{i,K}$ and T_K as quantities related to vertical fluxes induced by the eddies. Consider, say, the turbulent vertical flux of T , $\langle w'T' \rangle$, where w' and T' are the vertical velocity and T fluctuations, and $\langle \rangle$ denotes a time-average. In ODT this flux is calculated with

$$\langle w'T' \rangle = \frac{1}{\Delta t L} \sum_{eddie} l^2 T_K , \quad (6)$$

where \sum_{eddie} denotes summation over all the eddies implemented during the time interval Δt . It can be seen from (6) that larger (smaller) values of T_K are associated with a larger (smaller) vertical flux $\langle w'T' \rangle$.

2.4. Sampling of eddy events

Each event is characterized by a length scale l and a location z_0 which are randomly sampled from a joint probability density function $p(l, z_0; t)$ defined by

$$p(l, z_0; t) = \frac{\lambda(l, z_0; t)}{\int_0^L \int_0^L \lambda dl dz_0} . \quad (7)$$

$p(l, z_0; t) dl dz_0$ can be interpreted as the probability of occurrence of an eddy event of size within the range $[l, l + dl]$ with its lower boundary located within the range $[z_0, z_0 + dz_0]$. $\int_0^L \int_0^L \lambda dl dz_0$ is the overall event rate.

The eddy rate distribution λ is given by

$$\lambda = \frac{C}{l^3} \left[\sum_i u_{i,K}^2 + \frac{8}{27} glT_K - Z \left(\frac{\nu}{l} \right)^2 \right]^{1/2} , \quad (8)$$

if the expression inside the square root is positive, and $\lambda = 0$ otherwise. In (8), the summation is over the three velocity components, and C and Z are model parameters. Eddy events are sampled independently, but the time dependence of λ correlates these events in time. This feature of ODT generates an energy cascade (Kerstein 1999a). Physically, the eddy rate distribution incorporates into ODT the effects of temperature stratification, shear, and viscous damping on the turbulent fluctuations, with C determining the generation rate, i.e. C controls the strength of the turbulence. In (8), turbulent fluctuations can be generated by shear through $\sum_i u_{i,K}^2$, damped by viscous action through $-Z(\nu/l)^2$, and can be suppressed (enhanced) by the stable (unstable) temperature field through $(8/27)glT_K$.

2.5. Large-eddy-suppression mechanism

Consider an eddy event that has been sampled according to (7) and (8) and spans the range $[z_0, z_0 + l]$. The model formulated so far allows the occurrence of eddy events of size larger than the thickness of the mixing layer. This is unphysical because it violates scale locality. Therefore, the model includes the following steps to suppress these large eddy events. First, the range $[z_0, z_0 + l]$ is divided into three: $[z_0, z_0 + l/3]$, $[z_0 + l/3, z_0 + 2l/3]$, and $[z_0 + 2l/3, z_0 + l]$.

Then, λ is evaluated with (8) in each of these three intervals. Finally, if $\lambda = 0$ in any of these intervals, the eddy event is suppressed, otherwise, it is implemented. Among various proposed eddy suppression mechanisms (Kerstein *et al.* 2001, Ashurst and Kerstein 2005), this one is used here because it is deemed the least arbitrary.

2.6. Numerical implementation

The ODT model consists of the following components: the eddy operations (1); the sampling of eddy occurrence times and, using (7), eddy sizes and locations; the 1D equations for u_i and T ; the flow boundary and initial conditions; the discrete implementation of the 1D equations for u_i and T and of the eddy operations; the free parameters C and Z ; and the large-eddy suppression mechanism.

The 1D equations for u_i and T are

$$\frac{\partial u_i}{\partial t} = \nu \frac{\partial^2 u_i}{\partial z^2}, \quad (9a)$$

$$\frac{\partial T}{\partial t} = \kappa \frac{\partial^2 T}{\partial z^2} + R, \quad (9b)$$

where $R = 4T(1 - T)\tau_R^{-1}$. Zero-flux boundary conditions are applied to these equations:

$$\frac{\partial s}{\partial z} \Big|_{t,z=0} = \frac{\partial s}{\partial z} \Big|_{t,z=L} = 0, \quad (10)$$

where $s = u_i, T$. In addition, these boundary conditions are enforced by preventing triplet maps across $z = 0$ and $z = L$. The simulations are initialized with zero values for u_i and the following profile for T :

$$T(t = 0, z) = \frac{1}{2} - \frac{1}{2} \tanh \left(\frac{z - z_{f,0}}{\delta_T/2} \right),$$

where δ_T and $z_{f,0}$ are respectively the initial thickness and location of the fluids interface. We use an initial thickness of $\delta_T(Ag)^{1/3}\nu^{-2/3} \sim 1$, and $L(Ag)^{1/3}\nu^{-2/3} = 8000$ and $z_{f,0}L^{-1} = 1/2$ for the non-reactive case, and $L(Ag)^{1/3}\nu^{-2/3} = 24000$ and $z_{f,0}L^{-1} = 1/4$ for the reactive case. To avoid end-effects, the simulations are stopped long before the edges of the mixing layer get close (within $\sim 1000(Ag)^{-1/3}\nu^{2/3}$) to the domain boundaries. This is important for our current objectives.

Direct sampling of eddy events requires repeated reconstruction of the probability density function $p(l, z_0; t)$ as the flow evolves. This costly operation is avoided by using a Monte Carlo method called thinning (Law and Kelton 2000). The application of this method in ODT is described elsewhere (Kerstein 1999a, 2009, McDermott 2005). The 1D equations for u_i and T and the triplet map are implemented using a first-order finite-volume scheme with a non-uniform adaptive mesh (cf. Gonzalez-Juez *et al.* 2011a for more details). This approach allows accurate resolution of regions of the flow with very large property gradients. Within this framework, the flow property profiles within a given finite volume are uniform, and the finite volumes can be split, displaced, and merged. Time advancement is done using the forward Euler method. The ODT model is made dimensionless for numerical simulation by using $(Ag)^{-2/3}\nu^{1/3}$ as a time scale and $(Ag)^{-1/3}\nu^{2/3}$ as a length scale. However, in the following,

different quantities are made dimensionless using $(L/(Ag))^{1/2}$ as the time scale and $Ag t^2$ as the length scale. These dimensionless quantities are denoted with an asterisk.

3. Non-reactive Rayleigh-Taylor turbulent mixing

Rayleigh-Taylor mixing can be seen to occur in three stages (Youngs 1984): (i) initial perturbations grow exponentially in a way that can be analyzed with linear stability analysis; (ii) the instability saturates and longer wavelengths take over; and, (iii) a self-similar turbulent state is reached. ODT cannot capture 3D flow structures other than eddy events (triplet maps) and, therefore, it cannot be used to analyze stages (i)-(ii), or the effect of initial conditions. Hence the emphasis throughout is on stage (iii), Rayleigh-Taylor turbulence, and ODT results at early times (say $t(Ag)^{2/3}\nu^{-1/3} \lesssim 20$) are not discussed.

In the following, we compare ODT results for non-reactive Rayleigh-Taylor turbulence with DNS data. Even though there is abundant data on this problem (see citations of this paper for example), the DNS data of Vladimirova and Chertkov (2009) is used because, to our knowledge, this is the latest DNS of non-reactive Boussinesq Rayleigh-Taylor turbulence providing enough detail for the next comparison. The maximum value of the Reynolds number $4H(dH/dt)/\nu$, where H is a mixing layer width defined in section 3.1, is 13,000 in the DNS and 30,000 in the ODT simulations. We vary the model parameters of ODT in the ranges $3 \leq C \leq 20$ and $0.001 \leq Z \leq 0.1$. These ranges are selected because at smaller values of C or larger values of Z not enough eddy events are implemented, so that the flow is quasi-laminar, a condition of no interest here. Moreover, at larger values of C or smaller values of Z too many eddy events are implemented, making the simulations too expensive.

3.1. Temporal profiles

A usual observable in turbulent mixing is the width of the mixing layer. In Rayleigh-Taylor turbulence, this width has been defined in various ways. Here we use the same definition as in Vladimirova and Chertkov (2009) (cf. also Andrews and Spalding (1990)):

$$H = \int 4\langle T \rangle (1 - \langle T \rangle) dz, \quad (11)$$

where the brackets denote an average over at least 1000 realizations, and the integral is taken over the whole domain ($0 \leq z \leq L$). Figure 2 shows the temporal variation of H from ODT simulations at different values of C and Z , and that from DNS with different initial conditions. Notice in figure 2 the strong sensitivity of H to the ODT-model parameters C and Z : H increases more rapidly with time with increasing C , because the turbulence becomes stronger, and with decreasing Z , because the viscous damping is reduced, allowing more eddies to erode the edges of the mixing layer (cf. section 2.4). Also note in figure 2b that when the large-eddy-suppression mechanism is not used H increases very steeply and linearly with time. This unphysical result highlights the importance of using the large-eddy-suppression mechanism. More importantly, figure 2 shows that ODT simulations with $C = 5$ and $Z = 0.1$ produce a temporal evolution of H close to that of the DNS. These values of C and Z are used as base conditions in the remainder of this paper.

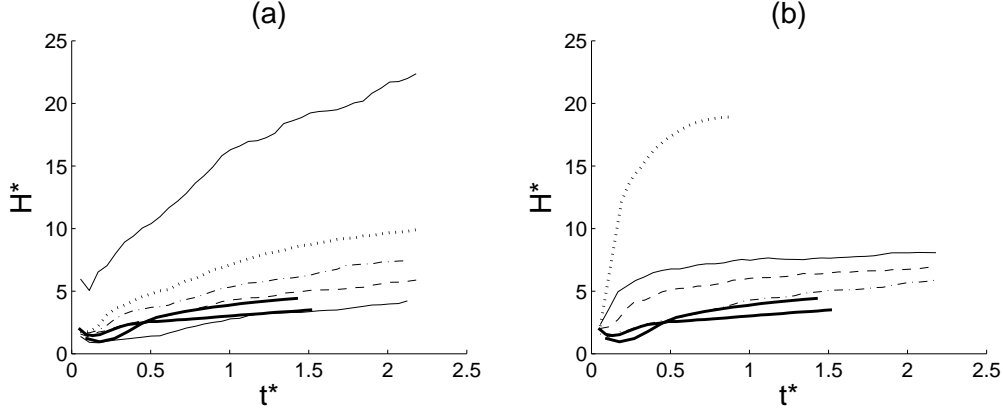


Figure 2. Temporal evolution of the width of the mixing layer H . (a) ODT results for $\tau_R = \infty$ (non-reactive case), $Z = 0.1$, and $C = 20$ (top thin solid line), 10 (dotted line), 7 (dashed-dotted line), 5 (dashed line), and 3 (bottom thin solid line). (b) ODT results for $\tau_R = \infty$, $C = 5$, and $Z = 0.001$ (thin solid line), 0.01 (dashed line), 0.1 (dashed-dotted line), and $Z = 0.1$ without the eddy suppression mechanism (dotted line). DNS data from Vladimirova and Chertkov (2009) for two different initial conditions are shown with thick solid lines.

Another key observable in turbulent mixing is a dimensionless parameter characterizing the growth of the mixing layer. In shear layers and wakes, ODT simulations give numerical values of such a parameter that depend on C and Z , and that can match those seen in DNS (Kerstein *et al.* 2001). Next, we show similar results for non-reactive Rayleigh-Taylor turbulence. In this type of flow, the dimensionless growth parameter is represented with α , and has been defined in different ways. A widespread definition is (Youngs 1984, 1989):

$$\alpha = \frac{H}{Ag t^2}, \quad (12)$$

with H taken in a visually pleasing portion of the data (Cabot and Cook 2006). The definition (12) is based on the self-similar scaling $H \sim Ag \Delta t^2$ (Youngs 1984). For the definition (12), DNS give $0.029 \leq \alpha \leq 0.040$ (Vladimirova and Chertkov 2009, Boffetta *et al.* 2010). In comparison, by fitting a parabola through the last portion ($t(Ag)^{2/3}\nu^{-1/3} \gtrsim 125$) of the curves in figure 2, ODT simulations give $0.02 \leq \alpha \leq 0.08$ for the different C and Z , and $\alpha = 0.03$ for the base conditions, which is close to DNS results. A more robust but less widespread definition of α is

$$\alpha = \frac{(dH/dt)^2}{4AgH}, \quad (13)$$

cf. Ristorcelli and Clark (2004). Figure 3 shows ODT results for the temporal evolution of α calculated with (13). The error bars denote the range of variation of α from the base conditions when C and Z are varied and other parameters are held constant. This notation for the error bars is used in subsequent figures. Notice in figure 3 that α reaches an approximately time-independent value for $C = 5$ and $Z = 0.1$ when $t(Ag)^{2/3}\nu^{-1/3} \gtrsim 125$, something which is also seen for other C and Z (not shown). More importantly, an approximately time-independent value of α is also observed in the DNS of Cabot and Cook (2006). (To be precise, towards the end of the simulation, the DNS of Cabot and Cook (2006) shows a very slight increase and then decrease of α .) This approximately time-independent α varies between $0.012 \leq \alpha \leq 0.056$

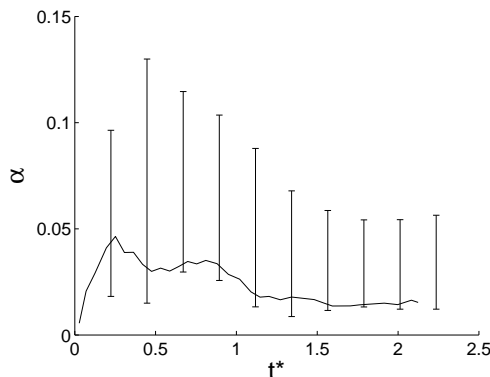


Figure 3. Temporal evolution of the growth parameter α for $\tau_R = \infty$ (non-reactive case), $C = 5$, and $Z = 0.1$. Error bars denote the range of variation of α from the base conditions when C and Z are varied and other parameters are held constant.

for different C and Z , and equals 0.015 for the base conditions, a value 25% less than that of 0.02 measured by Cabot and Cook (2006). We remark, however, that the DNS of Cabot and Cook (2006) is non-Boussinesq.

In Rayleigh-Taylor turbulence, approximately half of the change in potential energy per unit mass PE , defined as

$$PE = \frac{1}{L} \int \langle T(z, t = 0) - T(z, t) \rangle Agz dz , \quad (14)$$

is converted into kinetic energy per unit mass KE , defined as

$$KE = \frac{1}{2L} \sum_i \int u_{i,rms}^2 dz , \quad (15)$$

with the rest going into energy dissipation (Cabot and Cook 2006, Boffetta *et al.* 2010). This can be seen, for example, in figure 4, where the ratio KE/PE is close to 0.5, as observed previously (Youngs 1989, Ramaprabhu and Andrews 2003). Figure 4 indicates that ODT results are generally higher but trending toward agreement. It is not clear from the results shown in figure 4, however, if the ratio KE/PE reaches an asymptotic value. The presence or not of such a value is important because KE/PE times a factor is an upper bound for α (Youngs 1989, Dimonte *et al.* 2004).

The degree of mixing is characterized here with (Youngs 1984, Mueschke *et al.* 2006)

$$\theta = \frac{\langle T \rangle - \langle T^2 \rangle}{\langle T \rangle^2 - \langle T \rangle^2} , \quad (16)$$

with $\theta = 1$ indicating complete mixing. Previous studies show that the value of θ at the center of the mixing layer, $z = z_f$, with z_f given by

$$z_f = \int \langle T \rangle dz , \quad (17)$$

is in the range $0.75 \leq \theta \leq 0.8$ (Sharp 1984, Linden *et al.* 1994, Dimonte *et al.* 2004, Ramaprabhu and Andrews 2004). Figure 5 indicates that ODT values of θ tend to be lower.

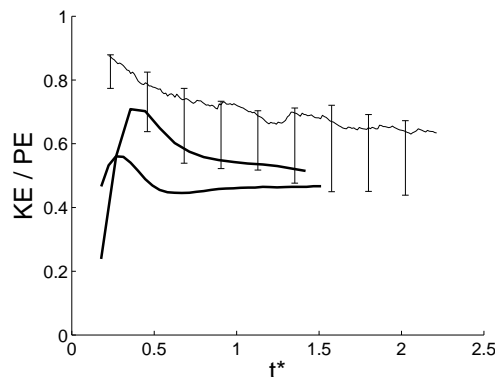


Figure 4. Temporal evolution of the ratio of kinetic energy and the change of potential energy KE/PE for $\tau_R = \infty$ (non-reactive case), $C = 5$, and $Z = 0.1$. ODT result is shown with a thin line and DNS results of Vladimirova and Chertkov (2009) with thick lines. The meaning of the error bars is the same as figure 3.

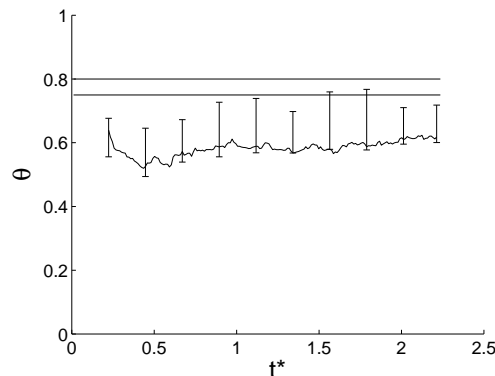


Figure 5. Temporal evolution of the degree of mixing θ at the center of the mixing layer ($z = z_f$) for $\tau_R = \infty$ (non-reactive case), $C = 5$, and $Z = 0.1$. The horizontal bars mark the range of results for θ obtained in various studies (Vladimirova and Chertkov 2009). The meaning of the error bars is the same as figure 3.

3.2. Spatial profiles and probability density functions

A more in-depth look at the mixing inside the mixing layer is provided by the PDF of T at the center of the mixing layer ($z = z_f$). Figure 6a shows that DNS and ODT results for this PDF agree fairly well when $0.1 \lesssim T \lesssim 0.9$. On the other hand, near $T \approx 1$ and $T \approx 0$, whereas the PDF approaches zero in the DNS, it increases abruptly in ODT simulations. These results indicate that while very little pure fluid (i.e., fluid with $T = 0$ or $T = 1$) travels through the center of the mixing layer in the DNS, more does in ODT. This artifact of ODT has been observed in simulations of planar shear layers and wakes (Kerstein *et al.* 2001). It happens because in ODT eddy events occur instantaneously and can bring pure fluid into the mixing layer from outside of it. By suppressing the eddy events bringing pure fluid near the center of the mixing layer, the PDF predicted by ODT better resembles that obtained in DNS, as can be seen in figure 6. This suppression mechanism, which is implemented in addition to that explained in section 2.5, discards eddies satisfying either one of the following conditions:

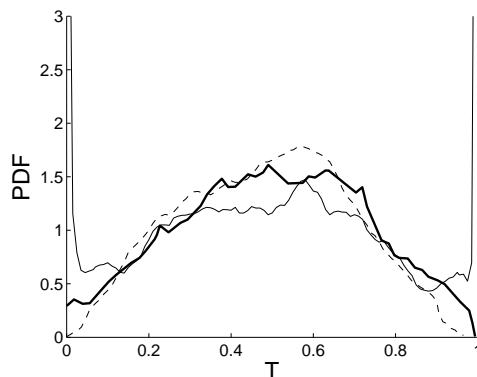


Figure 6. Probability density function of the temperature at the center of the mixing layer ($z = z_f$) towards the end of the simulation from ODT simulations with $\tau_R = \infty$, $C = 5$, $Z = 0.1$ (thin lines), and from the DNS of Vladimirova and Chertkov (2009) (thick solid line). ODT results without (solid line) and with (dashed line) the suppression of eddy events bringing pure fluid near the center of the mixing layer are shown.

$z_0 < z_f - 0.5h$ and $z_0 + l > z_f$, or $z_0 < z_f$ and $z_0 + l > z_f + 0.5h$. Here h is a mixing layer width defined by

$$h = 4 \int \langle T(1 - T) \rangle dz . \quad (18)$$

This suppression mechanism is not implemented in the baseline formulation of ODT because it is flow-specific, and it is preferable to avoid flow-specific modifications other than the adjustment of C and Z .

Another way of looking at the internal structure of the mixing zone is provided by the spatial profiles in the vertical direction presented in figures 7 and 8. Figure 7 shows, on the left, profiles of the mixing function $M = 4\langle T \rangle(1 - \langle T \rangle)$ from an ODT simulation at different times towards the end of the simulation ($175 < t(Ag)^{2/3}\nu^{-1/3} < 195$), and, on the right, profiles from DNS at the end of the simulation. In a similar way, figure 8 shows profiles of the rms velocity fluctuations $u_{i,rms}$. This way of presenting profiles of M and $u_{i,rms}$ is based on the symmetry of these profiles about the center plane $z = 0$ seen in both DNS and ODT (not shown). All velocity components are identical in ODT simulations of Rayleigh-Taylor turbulence. Hence only one velocity component is shown in figure 8. On the other hand, in DNS, vertical and horizontal velocity components are different, as can be seen in figure 8. Notice in figures 7 and 8 that z is made dimensionless with H , and $u_{i,rms}$ with $(AgH)^{1/2}$. These figures show that with this normalization profiles of M and $u_{i,rms}$ become self-similar at late times in ODT simulations, in agreement with DNS (Ristorcelli and Clark 2004, Vladimirova and Chertkov 2009). These profiles are also insensitive to C and Z (not shown). A close inspection of figure 7 reveals a slight difference between the profiles of M predicted by ODT and DNS. A greater difference can be seen in the profiles of $u_{i,rms}$ shown in figure 8. Notice in particular that, near the centerline, although ODT predicts a value of $u_{i,rms}$ within that of DNS, it produces an off-centerline peak not seen in the DNS. ODT simulations of shear layers also exhibit this behavior (Kerstein and Dreeben 2000, Kerstein *et al.* 2001). Such an off-centerline peak is also observed when using the eddy suppression mechanism discussed in the previous paragraph (not shown).

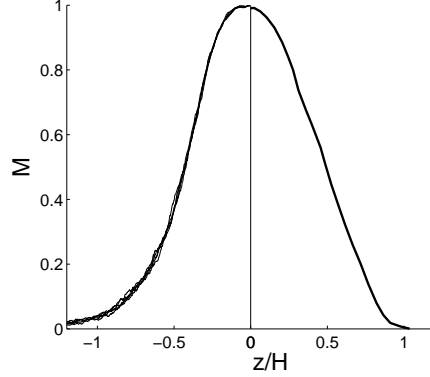


Figure 7. Vertical profiles of the mixing function $M = 4\langle T \rangle(1 - \langle T \rangle)$. ODT profiles for $\tau_R = \infty$ (non-reactive case), $C = 5$, and $Z = 0.1$ at different times towards the end of the simulation ($175 < t(Ag)^{2/3}\nu^{-1/3} < 195$) are shown on the left. DNS results of Vladimirova and Chertkov (2009) at the end of the simulation are shown on the right.

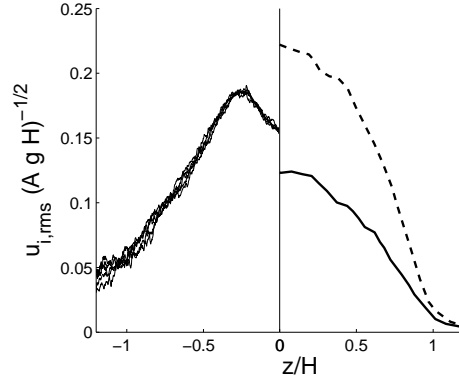


Figure 8. Vertical profiles of the rms velocity fluctuations. ODT profiles for $\tau_R = \infty$ (non-reactive case), $C = 5$, and $Z = 0.1$ at different times towards the end of the simulation ($175 < t(Ag)^{2/3}\nu^{-1/3} < 195$) are shown on the left. In the current formulation of ODT all velocity components are identical. DNS results for both the horizontal (solid line) and vertical (dashed line) velocity components at the end of the simulation are shown on the right.

4. Reactive Rayleigh-Taylor turbulent mixing

In reactive Rayleigh-Taylor mixing, the mixing layer or reaction zone between overlying heavy/cold reactants and underlying light/hot products moves against gravity, cf. figure 1 (Chertkov *et al.* 2009, Biferale *et al.* 2011). Hence the location of the reaction zone z_f , defined in equation (17), increases with time. Figure 9 indicates that ODT simulations capture this behavior. Only results for the base conditions ($C = 5$ and $Z = 0.1$) are shown in figure 9 and in subsequent ones.

4.1. Reduction in the growth of the reaction zone

Figure 10 shows the temporal evolution of the width of the reaction zone h , defined in equation (18). Here h is used instead of H because h predicts trends similar to H (not shown) and

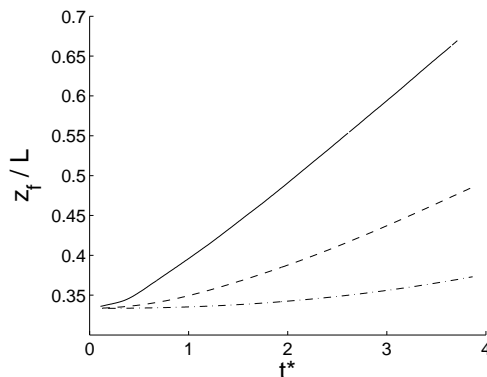


Figure 9. Temporal evolution of the reaction zone location z_f for $C = 5$, $Z = 0.1$ and $\tau_R = 10$ (solid lines), 100 (dashed lines), and 1000 (dashed-dotted lines).

it is easier to calculate. The main observation from figure 10 is that, at long enough times ($t > \tau_R$), whereas h increases with time in the non-reactive case and the reactive case with $\tau_R = 1000$, h decreases with time in other reactive cases.

Figure 10b shows that it is possible that the DNS simulations were not run long enough to observe the reduction in the growth of h . Running these simulations for times as long as those used with ODT would have been too computationally expensive. The reduced computational cost of ODT is what motivates its use in studies like the present one. It can also be seen in figure 10b that it is also possible that ODT simulations with $\tau_R = 1000$ were not run long enough to observe a reduced growth of h . Running such simulations would also have been too expensive, even for ODT.

The above-mentioned reduction of the growth of h is different from that documented by Khokhlov (1995) (cf. figure 9 of this paper). This is because, while the present simulations correspond to an unbounded horizontal domain, with no horizontal length scale entering the problem, those in Khokhlov (1995) involve a bounded horizontal domain, with a length scale that determines the scaling of h .

Heavy and light fluids are mixed by buoyancy in non-reactive Rayleigh-Taylor turbulence. In the reactive case, when these fluids are mixed, the reaction $R = 4T(1-T)\tau_R^{-1}$ can transform mixed fluid into light fluid. In other words, the reaction can separate the mixed fluid into heavy and light fluids. This mixing and separation can be analyzed using the PDF of T at $z = z_f$. Without reaction the PDF of T peaks around $0.4 \lesssim T \lesssim 0.6$, cf. figure 6, suggesting a well-mixed fluid. A similar result is observed with reaction when $t \lesssim \tau_R$ in both the DNS of Chertkov *et al.* (2009) and ODT simulations (not shown). The fluid separation is evident in both DNS and ODT when $t \gtrsim \tau_R$ in the form of two peaks, one near $T = 0$ and another one near $T = 1$, as shown in figure 11. It is evident that this interplay between buoyancy-induced mixing and reaction-induced separation is captured by ODT. The late-time transition to reduced growth of h indicated in figure 10 suggests that this separation dominates the mixing.

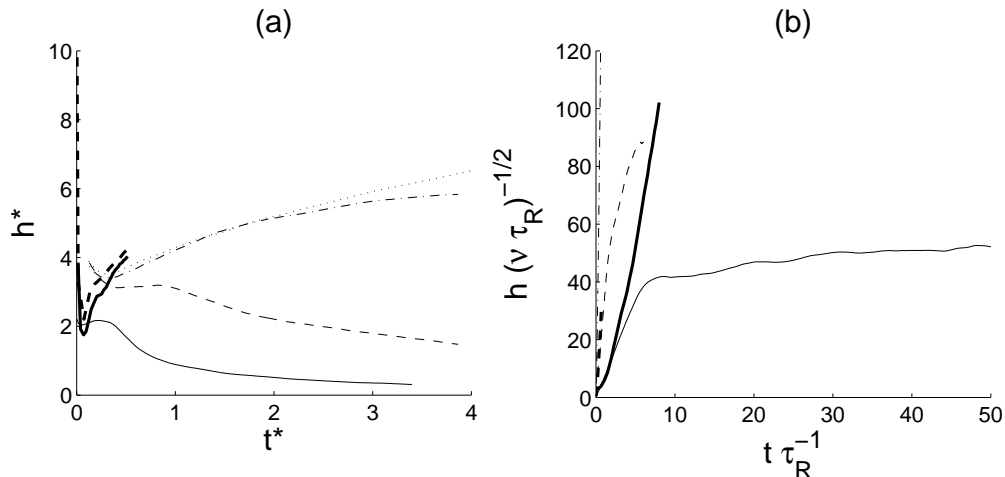


Figure 10. Temporal evolution of the width of the reaction zone h for $C = 5$, $Z = 0.1$ and $\tau_R = 10$ (thin solid lines), 100 (thin dashed lines), 1000 (thin dashed-dotted lines), and $\tau_R = \infty$ (thin dotted line in (a); collapses onto the vertical axis in (b)). DNS data from Chertkov *et al.* (2009) for H is shown for $\tau_R = 10$ (thick solid lines) and 112 (thick dashed lines).

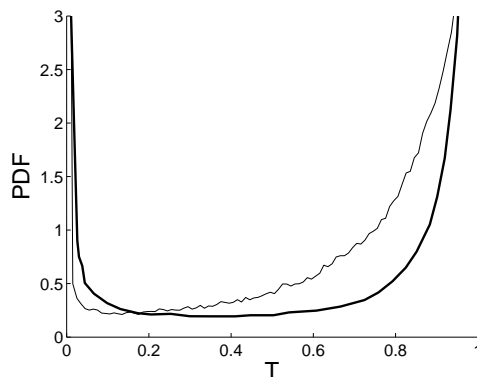


Figure 11. Probability density function of the temperature at the center of the mixing layer ($z = z_f$) near $t/\tau_R \approx 10$ from ODT simulations with $\tau_R = 100$, $C = 5$, $Z = 0.1$ (thin solid line), and from the DNS of Chertkov *et al.* (2009) (thick solid line).

4.2. Reactive Rayleigh-Taylor as a turbulent premixed flame problem

Next ODT results for reactive Rayleigh-Taylor turbulence are presented in the context of turbulent premixed combustion. This framework is useful to further analyze previous results. However, it should be kept in mind that the present problem is not a combustion process per se because there is not heat release. The relevance of the present work to combustion problems is the representation of mixing and flame-turbulence interactions in an idealized way.

Premixed combustion can be characterized by a Reynolds number Re , that represents the ratio of inertia to viscous forces, and a Damköhler number Da , representing the ratio of

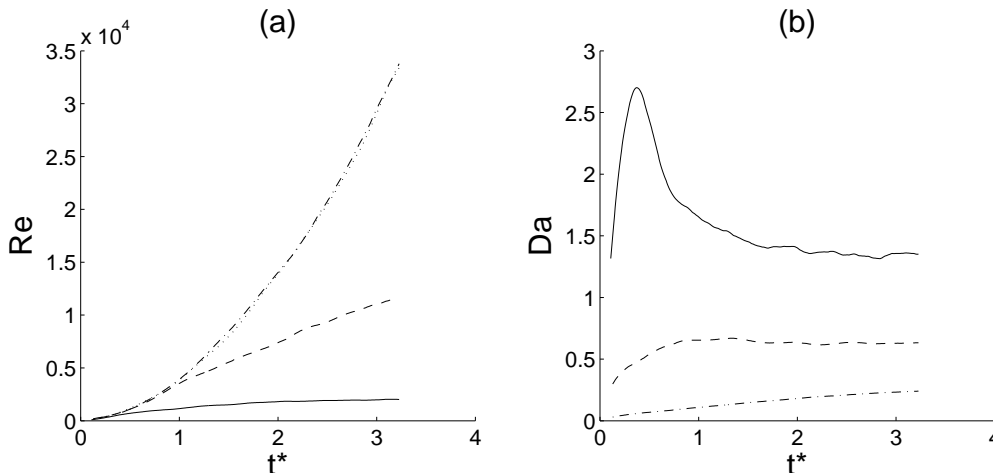


Figure 12. Temporal evolution of Re (a) and Da (b) for $C = 5$, $Z = 0.1$ and $\tau_R = 10$ (solid lines), 100 (dashed lines), 1000 (dashed-dotted lines), $\tau_R = \infty$ (dotted lines).

characteristic flow and chemical times. Here these dimensionless numbers are defined as

$$Re = \frac{u_{i,rms}(z = z_f)h}{\nu} \quad \text{and} \quad Da = \frac{h/u_{i,rms}}{\tau_R}. \quad (19)$$

A comparison of figures 10a and 12a reveal that the reduction of growth in h is accompanied by a reduction of the turbulence intensity, quantified here by Re . In other words, the separation process explained previously reduces the turbulence intensity. Additionally, figure 12b suggests that such growth reduction is also accompanied by a closer coupling between flow and “chemistry” (represented here in an idealized way here): For τ_R values of 100 and 10 but not 1000, Da is closer to one, which means that the characteristic time of the energetic eddies is about the same to that of the reaction, allowing flow and “chemistry” to interact.

The temporal evolution of Re and Da shown in figure 12 is used to produce the Re - Da plots presented in figure 13. Three different combustion regimes are identified in figure 13 (Turns 2000): a distributed-reactions regime, a reaction-sheets regime, and a flamelets-in-eddies regime. Notice that ODT results for reactive Rayleigh-Taylor turbulence are in the flamelets-in-eddies regime. In this regime parcels of gas that are not fully burned coexist with the burned gas (Turns 2000). As discussed earlier, a similar structure is seen at late times in reactive Rayleigh-Taylor turbulence, where parcels of pure heavy fluid and pure light fluid are observed at the center of the mixing layer.

Finally, figure 14 shows the scaling of the normalized turbulent flame speed $V_f/u_{i,rms}(z = z_f)$ with Da , where $V_f = dz_f/dt$. The observed linear scaling is consistent with $V_f = h/\tau_R$. This expression can be obtained by using equations (9) and its boundary conditions (10), the definitions (17) and (18), and by averaging over realizations and spatially integrating along z , cf. also Biferale *et al.* (2011).

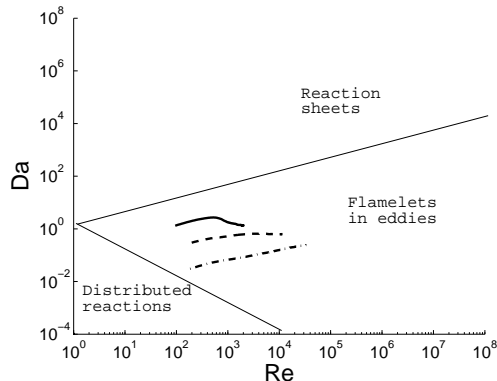


Figure 13. Re - Da plot showing different regimes in turbulent premixed combustion (taken from Turns (2000)) and data from ODT simulations of reactive Rayleigh-Taylor turbulence with $C = 5$, $Z = 0.1$ and $\tau_R = 10$ (solid lines), 100 (dashed lines), and 1000 (dashed-dotted lines).

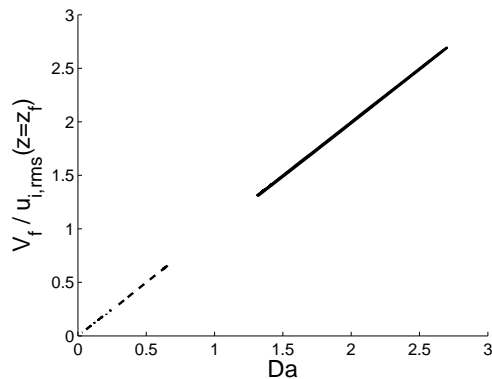


Figure 14. Scaling of the turbulent flame speed $V_f/u_{i,rms}(z=z_f)$ with Da for ODT simulations of reactive Rayleigh-Taylor turbulence with $C = 5$, $Z = 0.1$ and $\tau_R = 10$ (solid lines), 100 (dashed lines), and 1000 (dashed-dotted lines).

5. Summary and conclusions

- How do ODT results for non-reactive Rayleigh-Taylor turbulence compare with those from the DNS of Vladimirova and Chertkov (2009)? ODT predictions for global quantities—the growth of the mixing layer width α , the ratio of kinetic energy and change of potential energy KE/PE , and the degree of mixing θ —are within results observed in the DNS, with the precise comparison dependent on the choice of ODT parameter values. Hence ODT can be used to study global quantities in Rayleigh-Taylor turbulence. This gives us confidence in addressing the next question. ODT also agrees with DNS results in that, at long enough times, it produces self-similar spatial profiles of the mixing function M and rms velocity fluctuations $u_{i,rms}$. However, when looking at the internal structure of the mixing layer, ODT introduces two artifacts: First, pure fluid can go across the center of the mixing zone without mixing, and, second, velocity fluctuations exhibit an off-centerline peak. Hence ODT results for such internal structure should be interpreted with care.

- Can the reaction reduce the growth of the reaction zone in reactive Rayleigh-Taylor turbulence? ODT simulations show that if $t \gg \tau_R$ it is possible for the separation induced by the reaction to dominate the mixing produced by buoyancy, and abruptly reduce the growth of the reaction zone. Further investigation of this novel, though to some degree anticipated (Chertkov *et al.* 2009), behavior is warranted.
- What are the implications of the results of this paper for future work? This paper demonstrates the ability of ODT to capture the delicate interplay between buoyancy, turbulence, and reaction, and to address research questions that are difficult to address with other methods, such as DNS. Nonetheless, this work considers a very idealized problem: Reactive Rayleigh-Taylor turbulence in the Boussinesq framework, as defined in Chertkov *et al.* (2009). Therefore, future work with ODT should take the next step of considering a more complex framework that includes the effect of compressibility and uses a more realistic reaction, as done in Zingale *et al.* (2005) for example. An earlier form of ODT called the linear eddy model (LEM), which cannot capture buoyancy effects, has already been used to study supernova flames in this framework, but in the absence of gravity (Woosley *et al.* 2009, 2011).

Acknowledgments

This work was supported by the U.S. Department of Energy, Office of Basic Energy Sciences, Division of Chemical Sciences, Geosciences, and Biosciences. Sandia National Laboratories is a multi-program laboratory operated by Sandia Corporation, a Lockheed Martin Company, for the United States Department of Energy under contract DE-AC04-94-AL85000. Simulations were performed at Sandia National Laboratories on the Red Sky Linux Cluster.

References

- Abarzhi, S.I., Cadjan, M. and Fedotov, S., Stochastic model of Rayleigh-Taylor turbulent mixing. *Phys. Lett. A* 2007, **371**, 457–461.
- Abarzhi, S.I. and Rosner, R., A comparative study of approaches for modeling Rayleigh–Taylor turbulent mixing. *Phys. Scr.* 2010, **2010**, 014012.
- Andrews, M.J. and Spalding, D.B., A simple experiment to investigate two-dimensional mixing by Rayleigh–Taylor instability. *Phys. Fluids* 1990, **2**, 922.
- Ashurst, W.T. and Kerstein, A.R., One-dimensional turbulence: Variable-density formulation and application to mixing layers. *Phys. Fluids* 2005, **17**, 025107.
- Banerjee, A., Kraft, W. and Andrews, M., Detailed measurements of a statistically steady Rayleigh–Taylor mixing layer from small to high Atwood numbers. *J. Fluid Mech.* 2010, **659**, 127–190.
- Bell, J.B., Day, M.S., Rendleman, C.A., Woosley, S.E. and Zingale, M., Direct numerical simulations of type Ia supernovae flames. II. The Rayleigh–Taylor instability. *Astrophys. J.* 2004, **608**, 883–906.
- Biferale, L., Mantovani, F., Sbragaglia, M., Scagliarini, A., Toschi, F. and Tripiccone, R., Reactive Rayleigh–Taylor systems: front propagation and non-stationarity. *EPL* 2011, **94**, 54004.
- Boffetta, G., Mazzino, A., Musacchio, S. and Vozella, L., Statistics of mixing in three-dimensional Rayleigh–Taylor turbulence at low Atwood number and Prandtl number one. *Phys. Fluids* 2010, **22**, 035109.
- Cabot, W.H. and Cook, A.W., Reynolds number effects on Rayleigh-Taylor instability with possible implications for type Ia supernovae. *Nat. Phys.* 2006, **2**, 562–568.
- Chertkov, M., Lebedev, V. and Vladimirova, N., Reactive Rayleigh–Taylor turbulence. *J. Fluid Mech.* 2009, **633**, 1–16.
- Cook, A.W., Cabot, W. and Miller, P.L., The mixing transition in Rayleigh–Taylor instability. *J. Fluid Mech.* 2004, **511**, 333–362.

- Dimonte, G., Youngs, D.L., Dimits, A., Weber, S., Marinak, M., Wunsch, S., Garasi, C., Robinson, A., Andrews, M.J., Ramaprabhu, P. *et al.*, A comparative study of the turbulent Rayleigh–Taylor instability using high-resolution three-dimensional numerical simulations: the Alpha–Group collaboration. *Phys. Fluids* 2004, **16**, 1668–1693.
- Dreeben, T.D. and Kerstein, A.R., Simulation of vertical slot convection using one-dimensional turbulence. *Int. J. Heat Mass. Transf.* 2000, **43**, 3823–3834.
- Gonzalez-Juez, E.D., Kerstein, A.R. and Lignell, D.O., Fluxes across double-diffusive interfaces: a one-dimensional-turbulence study. *J. Fluid Mech.* 2011a, **677**, 218–254.
- Gonzalez-Juez, E.D., Kerstein, A.R. and Shih, L.H., Vertical mixing in homogeneous sheared stratified turbulence: a one-dimensional-turbulence study. *Phys. Fluids* 2011b, **23**, 055106.
- Kerstein, A.R., One-dimensional turbulence: Model formulation and application to homogeneous turbulence, shear flows, and buoyant stratified flows. *J. Fluid Mech.* 1999a, **392**, 277–334.
- Kerstein, A.R., One-dimensional turbulence: Part 2. Staircases in double-diffusive convection. *Dynam. Atmos. Oceans* 1999b, **30**, 25–46.
- Kerstein, A.R., One-dimensional turbulence: Stochastic simulation of multi-scale dynamics. *Lect. Notes Phys.* 2009, **756**, 291–333.
- Kerstein, A.R., Ashurst, W.T., Wunsch, S. and Nilsen, V., One-dimensional turbulence: Vector formulation and application to free shear flows. *J. Fluid Mech.* 2001, **447**, 85–109.
- Kerstein, A.R. and Dreeben, T.D., Prediction of turbulent free shear flow statistics using a simple stochastic model. *Phys. Fluids* 2000, **12**, 418–424.
- Kerstein, A.R. and Wunsch, S., Simulation of a stably stratified atmospheric boundary layer using one-dimensional turbulence. *Bound.-Lay. Meteorol.* 2006, **118**, 325–356.
- Khokhlov, A.M., Propagation of turbulent flames in supernovae. *Astrophys. J.* 1995, **449**, 695–713.
- Law, A.M. and Kelton, W.D., *Simulation Modeling and Analysis*, 2000 (McGraw-Hill).
- Linden, P.F., Redondo, J.M. and Youngs, D.L., Molecular mixing in Rayleigh–Taylor instability. *J. Fluid Mech.* 1994, **265**, 97–124.
- McDermott, R.J., Toward one-dimensional turbulence subgrid closure for large-eddy simulation. PhD thesis, University of Utah 2005.
- Mueschke, N.J., Andrews, M.J. and Schilling, O., Experimental characterization of initial conditions and spatio-temporal evolution of a small-Atwood-number Rayleigh–Taylor mixing layer. *J. Fluid Mech.* 2006, **567**, 27–63.
- Mueschke, N.J. and Schilling, O., Investigation of Rayleigh–Taylor turbulence and mixing using direct numerical simulation with experimentally measured initial conditions. I. Comparison to experimental data. *Phys. Fluids* 2009, **21**, 014106.
- Ramaprabhu, P. and Andrews, M., Simultaneous measurements of velocity and density in buoyancy-driven mixing. *Exp. Fluids* 2003, **34**, 98–106.
- Ramaprabhu, P. and Andrews, M.J., Experimental investigation of Rayleigh–Taylor mixing at small Atwood numbers. *J. Fluid Mech.* 2004, **502**, 233–271.
- Ristorcelli, J.R. and Clark, T.T., Rayleigh–Taylor turbulence: self-similar analysis and direct numerical simulations. *J. Fluid Mech.* 2004, **507**, 213–253.
- Sharp, D.H., An overview of Rayleigh–Taylor instability. *Physica D* 1984, **12**, 3–10.
- Tieszen, S.R., On the Fluid Mechanics of Fires. *Annu. Rev. Fluid Mech.* 2001, **33**, 67–92.
- Turns, S.R., *An Introduction to Combustion*, 2000 (McGraw-Hill).
- Vladimirova, N. and Chertkov, M., Self-similarity and universality in Rayleigh–Taylor, Boussinesq turbulence. *Phys. Fluids* 2009, **21**, 015102.
- Vladimirova, N., Constantin, P., Kiselev, A., Ruchayskiy, O. and Ryzhik, L., Flame enhancement and quenching in fluid flows. *Combust. Theory Modelling* 2003, **7**, 487–508.
- Woodsley, S.E., Kerstein, A.R. and Aspden, A.J., Flames in type Ia supernova: deflagration-detonation transition in the oxygen-burning flame. *Astrophys. J.* 2011, **734**, 37–41.
- Woodsley, S.E., Kerstein, A.R., Sankaran, V., Aspden, A.J. and Röpke, F.K., Type Ia supernova: calculations of turbulent flames using the linear eddy model. *Astrophys. J.* 2009, **704**, 255–263.
- Wunsch, S., Stochastic simulations of buoyancy-reversal experiments. *Phys. Fluids* 2003, **15**, 1442–1456.
- Wunsch, S. and Kerstein, A.R., A model for layer formation in stably stratified turbulence. *Phys. Fluids* 2001, **13**, 702–712.
- Wunsch, S. and Kerstein, A.R., A stochastic model for high-Rayleigh-number convection. *J. Fluid Mech.* 2005, **528**, 173–205.
- Youngs, D.L., Numerical simulation of turbulent mixing by Rayleigh–Taylor instability. *Physica D* 1984, **12**, 32–44.
- Youngs, D.L., Modelling turbulent mixing by Rayleigh–Taylor instability. *Physica D* 1989, **37**, 270–287.

Zingale, M., Woosley, S.E., Rendleman, C.A., Day, M.S. and Bell, J., Three-dimensional numerical simulations of Rayleigh–Taylor unstable flames in type Ia supernovae. *Astrophys. J.* 2005, **632**, 1021–1034.